Polymer 50 (2009) 2181–2189

Contents lists available at ScienceDirect

Polymer

journal homepage: www.elsevier.com/locate/polymer

# Numerical simulation of coil–helix transition processes of gelatin

Xiliang Chen [a], Yuxi Jia [a,*], Ligang Feng [a], Sheng Sun [a], Lijia An [b,*]

[a] School of Materials Science & Engineering, Shandong University, Jinan 250061, China
[b] State Key Laboratory of Polymer Physics and Chemistry, Changchun Institute of Applied Chemistry, Chinese Academy of Sciences, Changchun 130022, China

ARTICLE INFO

*Article history:*
Received 1 August 2008
Received in revised form
13 February 2009
Accepted 19 February 2009
Available online 5 March 2009

*Keywords:*
Structural inhomogeneity
Crosslinking density
Helix length

ABSTRACT

Gelatin is widely used in food, pharmaceutical, and photographic industries due to the coil–helix transition, whereas the structural inhomogeneity considerably affects its essential properties closely connecting with the industrial applications. The spatially structural inhomogeneity of the gelatin caused by the uneven and unstable temperature field is analyzed by the finite element method during the cooling-induced coil–helix transition process. The helix conversion and the crosslinking density as functions of time and spatial grid are calculated by the incremental method. A length distribution density function is introduced to describe the continuous length distributions of two kinds of triple helices. The results show that the crosslinking density and the length distribution of triple helices are dependent on the thermal histories. And the spatially structural inhomogeneity is more distinct when the initial gelatin concentration and the convective heat transfer coefficient increase. The present work is helpful for optimizing the fabrication conditions of gelatin.



## 1. Introduction

Gelatin is a kind of biopolymer made from collagen by hydrolytic degradation and widely used in food, pharmaceutical and photographic industries due to the coil–helix transition [1]. The coil–helix transition of gelatin has been studied by a number of researchers using various techniques such as X-ray diffraction, dynamic light scattering, transmission electron microscopy, rheo-optical measurements, Fourier transform mechanical spectroscopy, differential scanning calorimetry and nuclear magnetic resonance [1–29]. And various parameters are obtained by these researchers, such as the gel point, the helix amount, the viscosity below the gel point, the dynamic storage shear modulus, the dynamic loss shear modulus and the equilibrium shear modulus beyond the gel point.

The gelatin samples in the experiments mentioned above are generally considered to be homogeneous during the coil–helix transition process. In fact, due to the low thermal conductivity of gelatin [30], the temperature field of gelatin is commonly uneven and unstable, resulting in the structural inhomogeneity during the gelation process. The structural inhomogeneity considerably affects such physical properties as swelling, elasticity, permeability and transparency, which are the essential properties closely connecting with many industrial applications [31,32]. The study on the structural inhomogeneity of gelatin caused by the uneven and unstable temperature field has not been performed yet, though the studies on other gels have been reported [33–36]. Once the effects of the processing conditions on the structural inhomogeneity of the gels are known, the design of the gelatin fabrication process according to certain requirements can be done, as presented in Refs. [37,38].

The finite element method has been used in the study of both chemical gelation processes [39–43] and physical gelation processes [44–46]. In this paper, the numerical expressions of the kinetic model of the coil–helix transition of gelatin are constructed by the incremental method. On the basis of the temperature field simulated by the finite element method, the helix conversions and crosslinking density as functions of time and spatial grid are calculated, and then the length distributions of two kinds of triple helices are studied. Consequently the spatial difference of these structural parameters as a function of time is exhibited.

## 2. Construction of kinetic model of coil–helix transition

### 2.1. Renaturation mechanism

When the gelatin temperature decreases below the equilibrium melting point from a high temperature, the coil–helix transition would happen. By studying the reversion in very dilute rat-tail-tendon gelatin solutions, Flory and Weaver [11] proposed a two-step renaturation process, and postulated a transitory intermediate consisting of a single chain helix. The transformation may be represented as [11]

* Corresponding authors. Tel.: +86 531 88395811/431 85262206; fax: +86 531 88395811.
*E-mail addresses:* jia_yuxi@sdu.edu.cn (Y. Jia), ljan@ciac.jl.cn (L. An).

0032-3861/$ – see front matter © 2009 Elsevier Ltd. All rights reserved.
doi:10.1016/j.polymer.2009.02.039

$$C \underset{k_1}{\overset{k_1'}{\rightleftarrows}} I \underset{k_2}{\overset{k_2'}{\rightleftarrows}} (1/3)H \tag{1}$$

where C, I and H denote the random coil, the intermediate and the triple helix, respectively.

The second step is considerably faster than the first, and hence, the first step is the rate controlling. The rate of the transformation is determined by the gelatin concentration, $c$, and the rate constant, $k_1'$, as shown below [11]

$$k_1' = \text{Const.}\exp\left(\frac{-A}{kT\Delta T}\right) \tag{2}$$

where $A$ and $k$ denote constants, $T$ the transformation temperature, $\Delta T = T_m - T$ the degree of undercooling, and $T_m$ the equilibrium melting temperature.

Harrington and Rao [12] considered that if the helix strand is from one molecule, the kinetic model is first-order, from two molecules second-order, and three molecules third-order. Then Guo et al. [1] studied the initial renaturation process of bovine-bone gelatin solutions at semidilute concentrations from 2.5 to 119 kg/m$^3$ and over a temperature range from 3 to 30 °C, and proposed a new two-step mechanism: slow formation of a nuclear of two helical strands wrapping together, and rapid subsequent wrapping of another coil segment to form a triple helix. Hence, the first step is the rate controlling. In the first step, if the two strands of a nuclear are from a single chain with a loop, the kinetic model is first-order, while if from two chains without loop, it is second-order. In the second step, the wrapping coil segments may be from the same chains or the others, but the latter is much easier than the former, so the latter is predominant. So the final triple helices can be divided into single-looped and nonlooped triple helices corresponding to the first-order and second-order kinetics, respectively.

Recently, Gornall and Terentjev [7] discovered that the kinetics is strongly dependent on the temperature and concentration of the solvent, and proposed a first-order kinetic model. And they considered that the formation of triple helical nucleus occurs rapidly and the lengthening of the triple helices is predominant and rate limiting.

### 2.2. Kinetic equations of coil–helix transition

Guo et al. suggested a combination of first- and second-order kinetics, the kinetic equations of renaturation for the low concentration were proposed [1]

$$\frac{dX_1}{dt} = a(1 - \theta X_1 - \varphi X_2) \tag{3}$$

$$\frac{dX_2}{dt} = b(1 - \theta X_1 - \varphi X_2)^2 \tag{4}$$

by denoting

$$a = 0.018\,\frac{T}{\Delta T}\exp\left(-\frac{0.55T_m}{\Delta T}\right)$$

$$b = 0.003\,\frac{T}{\Delta T}\exp\left(-\frac{0.28T_m}{\Delta T}\right)c_0$$

$$\theta = 1 + \frac{2\pi R_l}{3l_1^*}$$

$$\varphi = 1 + \zeta \tag{5}$$

where $X_1$ and $X_2$ denote the helix fractions created by the first- and second-order reversions, respectively. $c_0$ denotes the initial gelatin concentration, and $R_1$ the radius of the end loop formed in the first-order renaturation. $l_1^*$ denotes the minimum stable length of the single-looped helices, which is dependent on the temperature. $\zeta$ denotes a universal constant, which is valid for all concentrations and temperatures. The value of the equilibrium melting temperature $T_m$ is considered to be constant, which is equal to 35 °C.

The analytical solution for this set of equations is given by Guo et al. when the gelatin temperature $T$ is constant, as shown below [1].

$$X_1 = -\frac{a^2\theta t}{b\varphi} + \frac{a}{b\varphi}\ln\left(\frac{(a\theta + b\varphi)\exp(a\theta t) - b\varphi}{a\theta}\right) \tag{6}$$

$$X_2 = \frac{1}{\varphi}\left(1 + \frac{a^2\theta^2 t}{b\varphi} - \frac{a\theta}{(a\theta + b\varphi)\exp(a\theta t) - b\varphi} - \frac{a\theta}{b\varphi} \times \ln\left(\frac{(a\theta + b\varphi)\exp(a\theta t) - b\varphi}{a\theta}\right)\right) \tag{7}$$

However, the temperature field in the coil–helix transition process is commonly uneven and unstable as a result of the low thermal conductivity of gelatin, especially when the sample size is large. Under the above-mentioned complicated condition, $a$, $b$ and $\theta$ are not constants, therefore Eqs. (6) and (7) cannot be used to calculate the helix conversion.

### 2.3. Numerical calculation of helix conversion

The complicated non-isothermal history can be divided into numerous time steps by the finite element method, resulting that each time step is short enough to be considered as an isothermal one. Hence, according to Eq. (5), the variables $a$, $b$ and $\theta$ in the kinetic equations can be considered to be constant in each time step.

In the first time step $\Delta t$ when the reversion starts, according to Eqs. (6) and (7), the conversions of single-looped and nonlooped triple helices, $X_{1(1)}$ and $X_{2(1)}$, can be calculated, respectively

$$X_{1(1)} = -\frac{a_{(1)}^2\theta_{(1)}\Delta t}{b_{(1)}\varphi} + \frac{a_{(1)}}{b_{(1)}\varphi} \times \ln\left(\frac{\left(a_{(1)}\theta_{(1)} + b_{(1)}\varphi\right)\exp\left(a_{(1)}\theta_{(1)}\Delta t\right) - b_{(1)}\varphi}{a_{(1)}\theta_{(1)}}\right) \tag{8}$$

$$X_{2(1)} = \frac{1}{\varphi}\left(1 + \frac{a_{(1)}^2\theta_{(1)}^2\Delta t}{b_{(1)}\varphi} - \frac{a_{(1)}\theta_{(1)}}{\left(a_{(1)}\theta_{(1)} + b_{(1)}\varphi\right)\exp\left(a_{(1)}\theta_{(1)}\Delta t\right) - b_{(1)}\varphi} - \frac{a_{(1)}\theta_{(1)}}{b_{(1)}\varphi}\ln\left(\frac{\left(a_{(1)}\theta_{(1)} + b_{(1)}\varphi\right)\exp\left(a_{(1)}\theta_{(1)}\Delta t\right) - b_{(1)}\varphi}{a_{(1)}\theta_{(1)}}\right)\right) \tag{9}$$

where the subscript (1) denotes being in the first time step.

At the time of $n\Delta t(n \geq 2)$, according to Eqs. (3) and (4), the helix conversions, $X_{1(n)}$ and $X_{2(n)}$, can be obtained by means of backward difference method and incremental method, as shown below

$$X_{1(n)} = a_{(n)}\Delta t\left(1 - \theta_{(n)}X_{1(n-1)} - \varphi X_{2(n-1)}\right) + X_{1(n-1)} \tag{10}$$

$$X_{2(n)} = b_{(n)}\Delta t\left(1 - \theta_{(n)}X_{1(n-1)} - \varphi X_{2(n-1)}\right)^2 + X_{2(n-1)} \tag{11}$$

where the subscript $(n-1)$ denotes being at the time of $(n-1)\Delta t$.

The minimum stable lengths of single-looped and nonlooped triple helices, $l^*_{1(n)}$ and $l^*_{2(n)}$, are calculated [1]

$$l^*_{1(n)} = -7.2\,\frac{kT_{(n)}T_m}{\Delta H \Delta T_{(n)}} \tag{12}$$

$$l^*_{2(n)} = -3.7\,\frac{kT_{(n)}T_m}{\Delta H \Delta T_{(n)}} \tag{13}$$

where $k$ denotes the universal constant of gas, and $\Delta H$ the enthalpy change per helix length when the helix is formed [28].

In Eqs. (10)–(13), the temperature as well as the undercooling degree in each time step is assumed to be constant. Therefore, according to Eq. (5), $a_{(n)}$, $b_{(n)}$ and $\theta_{(n)}$ in each time step are constants too.

The total helix conversion $X_{(n)}$ is

$$X_{(n)} = X_{1(n)} + X_{2(n)} \tag{14}$$

According to Eqs. (8)–(13), the conversions of single-looped and nonlooped triple helices can be numerically calculated under complicated non-isothermal conditions.

### 2.4. Numerical calculation of helix concentration

In the numerical calculation, the length of triple helices formed in one time step $\Delta t$ is assumed to be equivalent to the critical length of triple helices at the end of this time step and invariable once the triple helices are formed. In the first time step when the reversion starts, the concentrations of single-looped and nonlooped triple helices, $C_{1(1)}$ and $C_{2(1)}$, are calculated

$$C_{1(1)} = \frac{c_0 X_{1(1)}}{\rho l^*_{1(1)}} \tag{15}$$

$$C_{2(1)} = \frac{c_0 X_{2(1)}}{\rho l^*_{2(1)}} \tag{16}$$

where $\rho$ denotes the molar mass of unit length of triple helix.

The concentration increments of single-looped and nonlooped triple helices in the $n$th time step, $\Delta C_{1(n)}$ and $\Delta C_{2(n)}$, are calculated by backward difference method

$$\Delta C_{1(n)} = \frac{c_0\left(X_{1(n)} - X_{1(n-1)}\right)}{\rho l^*_{1(n)}} \tag{17}$$

$$\Delta C_{2(n)} = \frac{c_0\left(X_{2(n)} - X_{2(n-1)}\right)}{\rho l^*_{2(n)}} \tag{18}$$

At the time of $n\Delta t(n \geq 2)$, the concentrations of single-looped and nonlooped triple helices, $C_{1(n)}$ and $C_{2(n)}$, are calculated

$$C_{1(n)} = \sum_{i=1}^{n} \Delta C_{1(i)} \tag{19}$$

$$C_{2(n)} = \sum_{i=1}^{n} \Delta C_{2(i)} \tag{20}$$

Considering each triple helix is a crosslinking point, the total crosslinking density $C_{(n)}$ is

$$C_{(n)} = C_{1(n)} + C_{2(n)} \tag{21}$$

### 2.5. Governing equations of temperature field and boundary conditions

The governing equations of temperature field can be derived by functional analysis method or by weighted margin method. In the latter, Garlerkin method has been widely applied [47].

The coil–helix transition of gelatin is an exothermic process, but the thermal effect is very small, which can be neglected. When the coefficient of thermal conductivity $\lambda$, specific heat $c_p$ at constant pressure and gelatin density $\rho_g$ are regarded as constants, neglecting the internal heat source, the partial differential equation of temperature field in two-dimensional space can be obtained

$$D[T(x,y,t)] = \lambda\left(\frac{\partial^2 T}{\partial x^2} + \frac{\partial^2 T}{\partial y^2}\right) - \rho_g c_p \frac{\partial T}{\partial t} = 0 \tag{22}$$

The following control equation of temperature field is derived by Garlerkin method

$$\iint_D \left[\lambda\left(\frac{\partial W_l}{\partial x}\frac{\partial T}{\partial x} + \frac{\partial W_l}{\partial y}\frac{\partial T}{\partial y}\right) + \rho_g c_p W_l \frac{\partial T}{\partial t}\right] \mathrm{d}x\,\mathrm{d}y - \oint_\Gamma \lambda W_l \frac{\partial T}{\partial n}\,\mathrm{d}s = 0$$

$$(l = 1,2,\ldots,n;\ j = 1,2,\ldots,m) \tag{23}$$

where $W_l$ denotes the $l$th trial function, and $\Gamma$ the boundary of integral area.

Because of the temperature difference inside the cold atmosphere, there is natural convective heat transfer on the boundary between the gelatin and the cold atmosphere. Therefore, the thermal boundary condition of the gelatin and the cold atmosphere is the third kind of thermal boundary condition, as shown below [43]

$$-\lambda \left.\frac{\partial T}{\partial n}\right|_\Gamma = h\left(T - T_f\right)\Big|_\Gamma \tag{24}$$

where $h$ denotes the coefficient of convective heat transfer on the boundary between the gelatin and the cold atmosphere, and $T_f$ the temperature of the cold atmosphere.

The thermal boundary condition between the gelatin and the prototype (a mold core used to provide a specific shape for the gelatin part) is considered to be the special fourth kind of thermal boundary condition [43]. Namely, the heat-flow density $q_2$ through the interface is only determined by the heat conduction

$$q_2 = -\lambda \left.\frac{\partial T}{\partial n}\right|_\Gamma = h_c(T - T_{LOM})|_\Gamma \tag{25}$$

where $T_{LOM}$ denotes the temperature of the prototype, $h_c$ the coefficient of heat transfer on boundary between the gelatin and the prototype, and

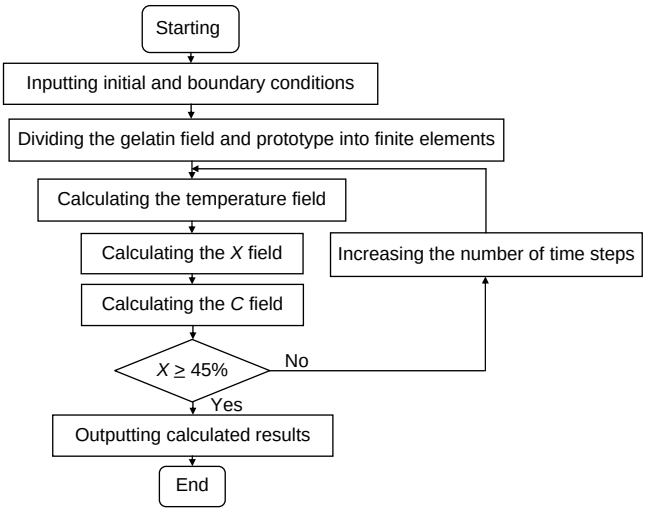


**Fig. 1.** Flow chart of the finite element simulation.

$$h_c = \frac{2\lambda \cdot \lambda_{LOM}}{L_g(\lambda + \lambda_{LOM})} \tag{26}$$

herein $\lambda_{LOM}$ denotes the coefficient of thermal conductivity of the prototype, and $L_g$ the surface roughness of the prototype.

## 3. Procedures of numerical simulation

The numerical simulation procedures are shown in Fig. 1.

Because at most 45% of gelatin can be converted to triple helices through the nucleation process [1], the calculation will be terminated when the helix conversion reaches 45%. For simplification of the numerical calculation, the effects of mass transfer process via convection and diffusion induced by temperature and concentration gradients are not taken into account in the simulation.

## 4. Simulated example

The shape of an example is shown in Fig. 2. Gelatin is in the outer layer, and a prototype is in the interior of the geometrical model. Since the geometrical model is symmetrical, a half of it (here left half) is calculated. The gelatin area is discretized to 136 elements with 163 nodes. The prototype area is discretized to 28 elements with 40 nodes. Four key nodes in the gelatin area are chosen, as shown in Fig. 2. Node A is on the corner of the gelatin, node B is on the edge of the gelatin, node C is in the interior of the gelatin, and node D is on the interface between the gelatin and the prototype. What should be noticed is that node C is one of the 163

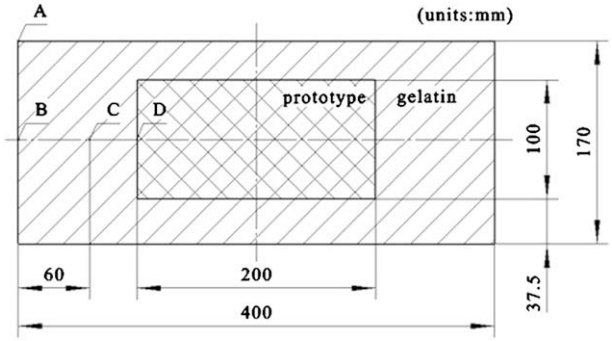


**Fig. 2.** Structure and dimensions of calculated example.

**Table 1**
Key input data.

| Parameters | Numerical values |
|---|---|
| Density of gelatin system when $c_0 = 50.8$ kg/m$^3$ | 1016 kg/m$^3$ |
| Specific heat of gelatin system | 4.174 kJ/(kg K) |
| Coefficient of thermal conductivity of gelatin system | 0.1858 W/(m K) [30] |
| Volume specific heat of prototype | 2000 kJ/(m$^3$ K) |
| Coefficient of thermal conductivity of prototype | 0.01 W/(m K) |
| Surface roughness of prototype | 0.0001 m |
| Coefficient of convective heat transfer | 6 W/(m$^2$ K) |

nodes, whose distance to the edge is just 60 mm. So the four nodes can be regarded as the representatives of the gelatin area, and the discussions on the evolutions of key variables will be focused on these four nodes.

The initial temperature of the example is 45 °C, located in the cold atmosphere with the temperature of 20 °C. The main input parameters are listed in Table 1.

## 5. Results and discussions

The helix conversion is a key variable denoting the degree of the cooling-induced coil–helix transition [1,11–13,16–19]. The sum of the concentration of two kinds of triple helices is the crosslinking density, which is an important variable closely connecting with the gel mechanical properties [40–43]. The triple helix length considerably affects the elasticity of gelatin [48]. So the evolutions of the key variables on different nodes are studied in sequence.

### 5.1. Evolution of gelatin temperature

The curves of gelatin temperature versus time are shown in Fig. 3. At the initial stage, the cooling rates of the surface nodes of the gelatin are larger than those of the interior nodes due to the heat resistance of the gelatin. At the latter stage, the cooling rates of all these nodes decrease because the temperature difference between the gelatin and the atmosphere becomes smaller with the time increasing. At last, the temperature of the gelatin is almost the same as that of the atmosphere. The phenomenon revealed by the simulation results is in agreement with the basic law of heat transfer.

### 5.2. Evolution of helix conversion

The curves of helix conversion versus time are shown in Fig. 4. The coil–helix transition occurs first on node A, which is followed

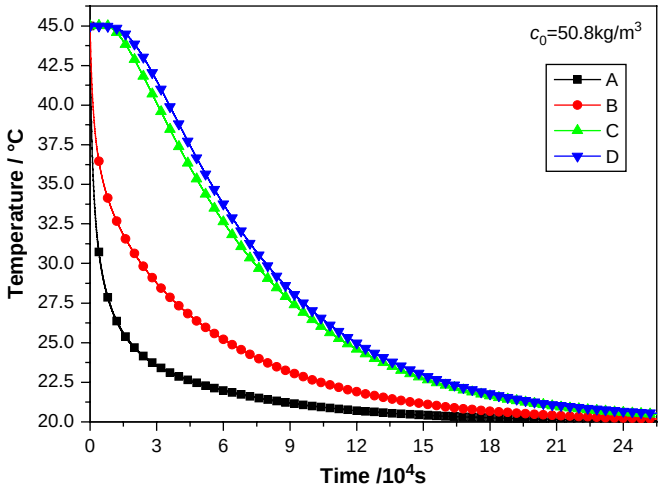


**Fig. 3.** Curves of gelatin temperature versus time on four different nodes A, B, C, and D.

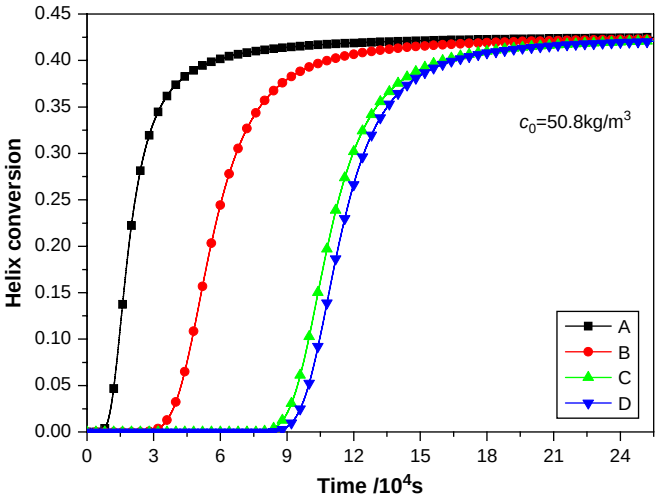


**Fig. 4.** Curves of helix conversion versus time on four different nodes A, B, C, and D.

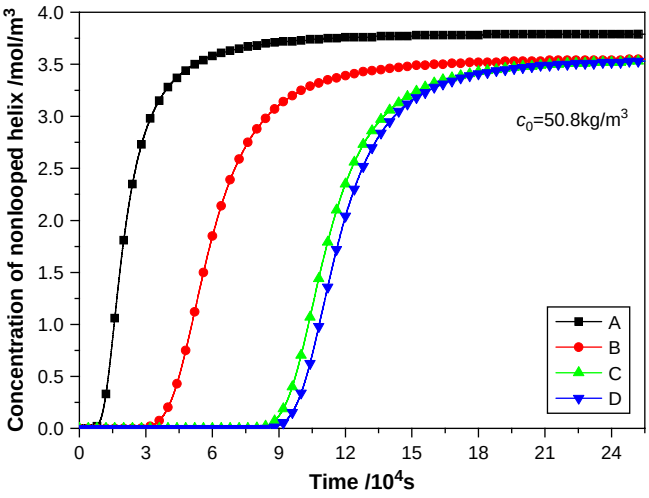


**Fig. 6.** Curves of nonlooped triple helix concentration versus time on four different nodes A, B, C, and D.

by nodes B, C, and D. The reason is as follows. As shown in Fig. 3, at the initial stage, the temperature of the gelatin does not decrease to the equilibrium melting temperature $T_m$, and the coil–helix transition does not occur at the moment. The temperature of the gelatin decreases gradually with the time increasing, and the cooling rate of node A is larger than that of others. Therefore, the temperature of node A can reach the equilibrium melting temperature first, and then the coil–helix transition occurs first on node A.

As shown in Fig. 4, for each node, the change rate, $\partial X/\partial t$, of the helix conversion increases gradually with the time increasing at the initial stage, and decreases at the latter stage. Eventually, the helix conversion tends to a constant. The evolution characteristics can be explained by the following analysis. The lower the temperature of the gelatin is, the more easily the coil–helix transition occurs. At the initial stage, the change rate of the helix conversion increases gradually with the time increasing because of the decreasing of the gelatin temperature. At the latter stage, according to Eqs. (10), (11) and (14), the coils that could form triple helices become less and less. So the change rate of the helix conversion decreases with the time increasing at the latter stage.

The simulation results are compared with experimental ones as follows. In Ref. [29], the gelation process of several kinds of gelatin is studied experimentally using small samples under non-isothermal conditions, in which the so-called "A1" gelatin is the same as the one used in this paper. It can be seen that the temperature curve of node A in Fig. 3 is similar to that in Illustration 3 in Ref. [29], and that the helix conversion curve of node A in Fig. 4 is also similar to the one of "A1" gelatin shown in Illustration 3 in Ref. [29]. So it can be concluded that the simulation results of the helix conversion obtained from the temperature histories are reasonable.

### 5.3. Evolution of crosslinking density

The curves of crosslinking density versus time are shown in Fig. 5, whose evolution trend is similar to that of Fig. 4. For each node, the change rate of the crosslinking density, $\partial C/\partial t$, increases gradually with the time increasing at the initial stage, while decreases at the latter stage. The reason is as follows. At the initial stage, the decreasing of the gelatin temperature induces that the critical helix length becomes shorter with the time increasing, which can be concluded from Eqs. (12) and (13). In addition, the change rate of the helix conversion increases at the initial stage, as shown in Fig. 4. Therefore, according to Eqs. (15)–(18), it can be concluded that the change rate of the crosslinking density increases

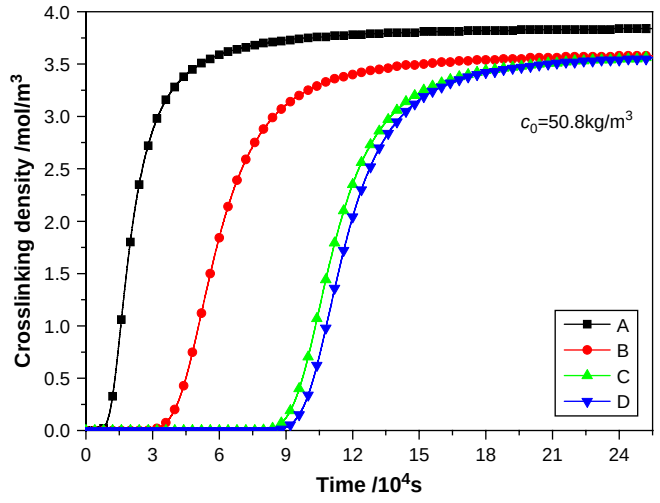


**Fig. 5.** Curves of crosslinking density versus time on four different nodes A, B, C, and D.

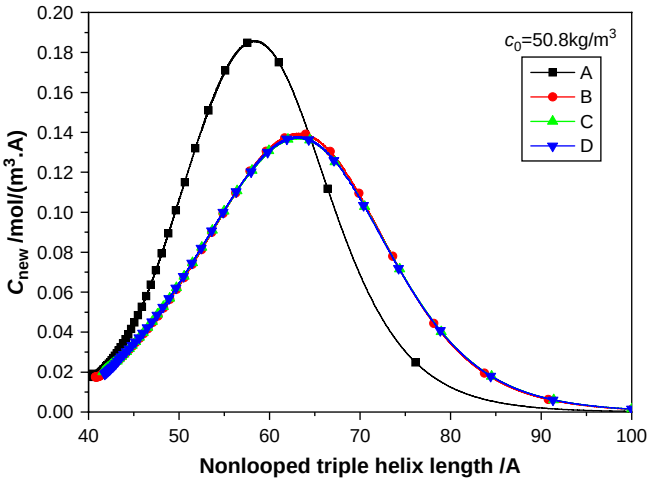


**Fig. 7.** Length distributions of nonlooped triple helices at the time of $2.55 \times 10^5$ s on four different nodes A, B, C, and D.

**Table 2**
Calculated results of $\overline{L}_n$, $\overline{L}_w$, and $\overline{L}_w/\overline{L}_n$ of nonlooped triple helices on four different nodes A, B, C, and D.

| | A | B | C | D |
|---|---|---|---|---|
| $\overline{L}_n$/Å | 59.63 | 63.38 | 63.74 | 63.74 |
| $\overline{L}_w$/Å | 60.62 | 65.33 | 65.33 | 65.33 |
| $\overline{L}_w/\overline{L}_n$ | 1.017 | 1.031 | 1.025 | 1.025 |

with the time increasing at the initial stage. At the latter stage, although the critical helix length still decreases with the time increasing, the decrease of the change rate of the helix conversion is predominant. Hence, the change rate of the crosslinking density decreases with the time increasing at the latter stage. Finally, the crosslinking density approaches a constant.

There is a distinct difference between Figs. 4 and 5 at the latter stage, namely, the crosslinking density of node A in Fig. 5 is significantly higher than that of others. The phenomenon is explained below. A larger cooling rate of node A leads to a larger undercooling degree than that of others. Therefore, the length of the triple helices formed on node A is shorter than that on other nodes, which can be concluded from Eqs. (12) and (13). And as shown in Fig. 4, the helix conversions of the four nodes at the end of horizontal abscissa ($2.55 \times 10^5$ s) are almost the same. Consequently, a higher crosslinking density of node A is obtained eventually.

### 5.4. Numerical analysis of key variables of nonlooped triple helices

#### 5.4.1. Evolution of nonlooped triple helix concentration

The curves of nonlooped triple helix concentration versus time are shown in Fig. 6. Similar to Fig. 5, for each node, the change rate of the nonlooped triple helix concentration, $\partial C_2/\partial t$, increases gradually with the time increasing at the initial stage, and decreases at the latter stage. Also the nonlooped triple helix concentration of node A is significantly higher than that of others.

#### 5.4.2. Length distribution of nonlooped triple helices

As mentioned in Section 2.4, the length of triple helices formed in one time step is assumed to be equivalent to the critical length of triple helices at the end of this time step. In the paper, $L_k$ is used to denote the helix length in the $k$th ($k \geq 1$) time step, and $L_{k+1}$ is used to denote the helix length in the next time step. Because of the cooling characteristics, according to Eqs. (12) and (13), $L_{k+1} < L_k$. By this means, the calculated helix lengths as well as the corresponding concentrations are discrete, which is attributed to the inherent discreteness characteristics of the numerical calculation.

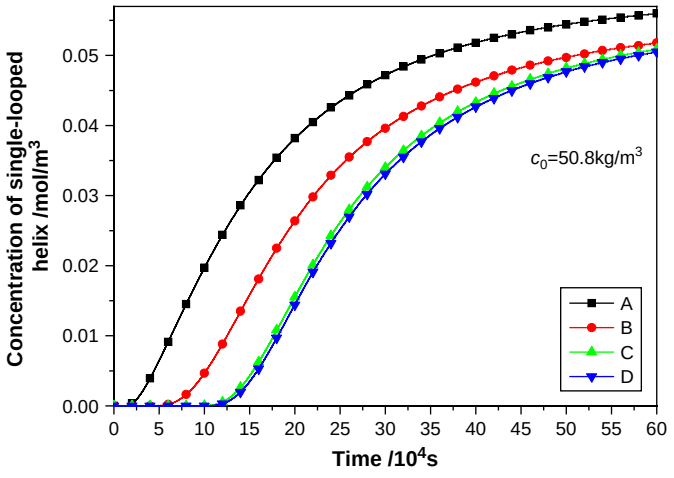


**Fig. 8.** Curves of single-looped triple helix concentration versus time on four different nodes A, B, C, and D.

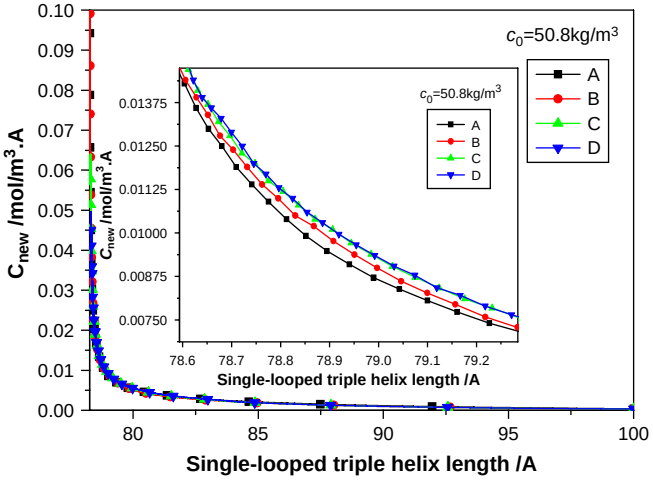


**Fig. 9.** Length distributions of single-looped triple helices at the time of $6 \times 10^5$ s on four different nodes A, B, C, and D.

To describe the continuous distribution of the triple helix length, a length distribution density function is introduced and defined as

$$C_{new} = \frac{\Delta C_{(k)}}{L_k - L_{k+1}} \tag{27}$$

where $\Delta C_{(k)}$ denotes the concentration of the triple helices with the length $L_k$. Obviously, the unit of measure for $C_{new}$ is mol/($m^3$ Å).

The length distributions of nonlooped triple helices at the time of $2.55 \times 10^5$ s are shown in Fig. 7. For node A, $C_{new}$ has a maximum value at around 58 Å. But for nodes B, C, and D, $C_{new}$ reaches the maximum at about 63 Å. Namely, the helix length corresponding to the peak of node A is shorter than that of others. The phenomenon is explained below. As mentioned above, the length of the nonlooped triple helices formed on node A is shorter than that on other nodes, resulting in the length of nonlooped triple helices on node A concentrating on the shorter one than that on others. What should be noticed is that the integrals of the curves in Fig. 7 are equal to the values of the nonlooped triple helix concentrations at the time of $2.55 \times 10^5$ s in Fig. 6.

It can be seen from Fig. 7 that the shortest length of the nonlooped triple helices is about 40 Å. The result accords with the length of the nonlooped triple helices under the quench temperature 20 °C, as shown in Illustration 11 in Ref. [1].

#### 5.4.3. Average length of nonlooped triple helices

Modeling on the definition of number average molecular weight and weight average molecular weight, the number average helix length and the weight average helix length are calculated, respectively

**Table 3**
Calculated results of $\overline{L}_n$, $\overline{L}_w$, and $\overline{L}_w/\overline{L}_n$ of single-looped triple helices on four different nodes A, B, C, and D.

| | A | B | C | D |
|---|---|---|---|---|
| $\overline{L}_n$/Å | 84.29 | 84.36 | 84.48 | 84.55 |
| $\overline{L}_w$/Å | 84.96 | 85.13 | 85.12 | 85.48 |
| $\overline{L}_w/\overline{L}_n$ | 1.008 | 1.009 | 1.008 | 1.011 |

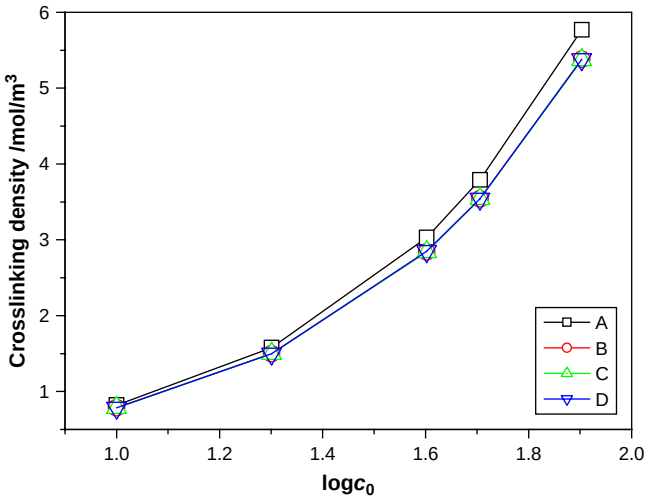


**Fig. 10.** Curves of crosslinking density versus log $c_0$ when helix conversion is 42% on four different nodes A, B, C, and D.

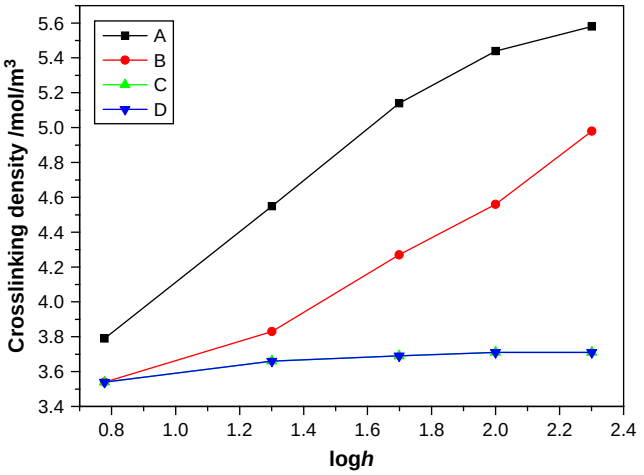


**Fig. 11.** Curves of crosslinking density versus log $h$ when helix conversion is 42% on four different nodes A, B, C, and D.

$$\overline{L}_n = \frac{\sum_i L_i \Delta C_{(i)}}{\sum_i \Delta C_{(i)}} \tag{28}$$

$$\overline{L}_w = \frac{\sum_i L_i L_i \Delta C_{(i)}}{\sum_i L_i \Delta C_{(i)}} \tag{29}$$

where $\overline{L}_n$ and $\overline{L}_w$ denote the number average helix length and the weight average helix length, respectively.

At the time of $2.55 \times 10^5$ s, the values of $\overline{L}_n$ and $\overline{L}_w$, as well as the polydispersity index $\overline{L}_w/\overline{L}_n$ of nonlooped triple helices on nodes A, B, C, and D are listed in Table 2, from which it can be seen that the nonlooped triple helix length has a narrow polydispersity.

### 5.5. Numerical analysis of key variables of single-looped triple helices

#### 5.5.1. Evolution of single-looped triple helix concentration

The curves of single-looped triple helix concentration versus time are shown in Fig. 8. Similar to Figs. 5 and 6, for each node, the change rate of the single-looped triple helix concentration, $\partial C_1/\partial t$, increases gradually with the time increasing at the initial stage, and decreases at the latter stage. Also the single-looped triple helix concentration of node A is significantly higher than that of others. The reason is the same as that above-mentioned.

In Figs. 3–6, the end time is $2.55 \times 10^5$ s. While in Fig. 8, the end time is $6 \times 10^5$ s. The reason is as follows. At the time of $2.55 \times 10^5$ s, the curves in Figs. 3–6 have already tended to be stable, but the curves in Fig. 8 have not tended to be stable. And if a longer time than $6 \times 10^5$ s is taken, the data in Fig. 8 will not be accurate due to the accumulated error caused by the inherent limitation of the numerical calculation. So the end time in Fig. 8 is taken as $6 \times 10^5$ s.

**Table 4**
Convective heat transfer mode and its relevant numerical range [49].

| Courses | $h$/[W/(m$^2$ K)] |
|---|---|
| *Natural convection* | |
| Atmosphere | 1–10 |
| Water | 200–1000 |
| *Forced convection* | |
| Atmosphere | 20–100 |
| High-pressure steam | 500–35,000 |
| Water | 1000–1500 |

#### 5.5.2. Length distribution of single-looped triple helices

The length distributions of single-looped triple helices at the time of $6 \times 10^5$ s are shown in Fig. 9. For nodes A, B, C, and D, the trends of the curves are basically the same and monotonically increasing with the decrease of the single-looped triple helix length. The reason is as follows. When the transition time approaches $6 \times 10^5$ s, the gelatin temperature tends to be stable, and is very close to the cold atmosphere temperature 20 °C. Hence, the length of the newly formed single-looped triple helices also tends to the critical helix length at the temperature of 20 °C.

The result that $C_{new}$ diverges reveals a higher decrease order of the difference between $L_k$ and $L_{k+1}$ comparing with that of $\Delta C_{(k)}$ when approaching the time of $6 \times 10^5$ s.

As shown in Fig. 9, the shortest length of the single-looped triple helices is about 78 Å, which is in agreement with the length of the single-looped triple helices under the quench temperature 20 °C shown in Illustration 11 in Ref. [1].

#### 5.5.3. Average length of single-looped triple helices

At the time of $6 \times 10^5$ s, the number average length and the weight average length, $\overline{L}_n$ and $\overline{L}_w$, as well as the polydispersity index $\overline{L}_w/\overline{L}_n$ of single-looped triple helices on nodes A, B, C, and D are listed in Table 3. Similar to Table 2, the single-looped triple helix length also has a narrow polydispersity.

### 5.6. Effect of initial collagen concentration on crosslinking density

The initial collagen concentration $c_0$ is changed for calculation while other conditions are kept constant, as listed in Table 1. The values of $c_0$ are set as 10, 20, 40, 50.8, and 80 kg/m$^3$, respectively. All these values are suitable for the equations used for the simulation.

It can be seen from Fig. 4 that when the helix conversion is 42%, the coil–helix transition has tended to be stable. Hence, when the helix conversion is 42%, the curves of crosslinking density versus log $c_0$ are shown in Fig. 10.

It can be seen from Fig. 10 that the crosslinking density increases with the increasing of $c_0$, which can be explained by the following analysis. The larger the value of $c_0$ becomes, the more molecules that could form helices exist, and consequently, the larger value of crosslinking density is obtained.

### 5.7. Effect of convective heat transfer coefficient on crosslinking density

The convective heat transfer coefficient, $h$, on the boundary between the gelatin and the cold atmosphere is changed for calculation while other conditions are kept constant, as listed in Table 1. The values of $h$ in calculations are set as 6, 20, 50, 100, and 200 W/(m$^2$ K), respectively. The convective heat transfer mode and its relevant numerical range are listed in Table 4.

Similar to Fig. 10, when the helix conversion is 42%, the curves of crosslinking density versus log $h$ are shown in Fig. 11. The crosslinking density of node A as well as node B increases with the increasing of the value of $h$, while the crosslinking density of node C as well as node D does not change significantly with the increasing of the value of $h$. The reason is analyzed below. Nodes A and B are on the surface of the gelatin, where a direct convective heat transfer occurs. The larger the value of $h$ becomes, the larger the cooling rate of nodes A and B is, and then the shorter the length of the formed triple helices is. In addition, the helix conversion is 42% for all the cases. Therefore, the crosslinking density of nodes A and B increases with the increasing of the value of $h$. While nodes C and D are the interior nodes, and the thermal conductivity of the gelatin is low. So the response of nodes C and D to the change of the cold atmosphere is slow, namely, the change of $h$ has very little effect on the interior nodes.

## 6. Conclusions

The spatially structural inhomogeneity of gelatin is numerically analyzed during the cooling-induced coil–helix transition process. The crosslinking density and the length distribution of triple helices are found to be dependent on the thermal histories. The crosslinking density on the surface of gelatin is larger than the inner one at the end of transition. The polydispersity of the triple helix length on the surface of gelatin is narrower than the inner one, and the average length of triple helices on the surface is shorter than the inner one. The spatially structural inhomogeneity is more distinct when the initial gelatin concentration and the convective heat transfer coefficient increase.

The comparisons with the experimental results show that the calculated results are reasonable. The present work is helpful for optimizing gelatin fabrication conditions, and then the design of the coil–helix transition process according to certain requirements can be done.

In relation to actual applications, the material of the prototype may be changed easily, and then the parameter of heat transfer coefficient ($h_c$) between the gelatin and prototype should be examined, so the effect of $h_c$ on the crosslinking density should be considered.

## Acknowledgements

This work is supported by the National Natural Science Foundation of China (50621302, 20734003, 20620120105) Programs.

## References

[1] Guo L, Colby RH, Lusignan CP, Whitesides TH. Kinetics of triple helix formation in semidilute gelatin solutions. Macromolecules 2003;36:9999–10008.
[2] Pezron I, Djabourov M, Bosio L, Leblond J. X-ray diffraction of gelatin fibers in the dry and swollen states. Journal of Polymer Science, Part B: Polymer Physics 1990;28:1823–39.
[3] Matsunaga T, Shibayama M. Gel point determination of gelatin hydrogels by dynamic light scattering and rheological measurements. Physical Review E 2007;76:030401(4).
[4] Djabourov M, Bonnet N, Kaplan H, Favard N, Favard P, Lechaire JP, et al. 3D analysis of gelatin gel networks from transmission electron microscopy imaging. Journal de Physique II 1993;3:611–24.
[5] Guo L, Colby RH, Lusignan CP, Howe AM. Physical gelation of gelatin studied with rheo-optics. Macromolecules 2003;36:10009–20.
[6] Gornall JL, Terentjev EM. Concentration–temperature superposition of helix folding rates in gelatin. Physical Review Letters 2007;99:028304(4).
[7] Gornall JL, Terentjev EM. Universal kinetics of helix–coil transition in gelatin. Physical Review E 2008;77:031908(8).
[8] Hawkins K, Lawrence M, Williams PR, Williams RL. A study of gelatin gelation by Fourier transform mechanical spectroscopy. Journal of Non-Newtonian Fluid Mechanics 2008;148:127–33.
[9] Cuppo F, Venuti M, Cesaro A. Kinetics of gelatin transitions with phase separation: T-jump and step-wise DSC study. International Journal of Biological Macromolecules 2001;28:331–41.
[10] Brand T, Richter S, Berger S. Diffusion NMR as a new method for the determination of the gel point of gelatin. Journal of Physical Chemistry B 2006;110:15853–7.
[11] Flory PJ, Weaver ES. Helix–coil transitions in dilute aqueous collagen solutions. Journal of the American Chemical Society 1960;82:4518–25.
[12] Harrington WF, Rao NV. Collagen structure in solution. I. Kinetics of helix regeneration in single-chain gelatins. Biochemistry 1970;9:3714–24.
[13] Ter Meer HU, Lips A, Busnel J-P. In: Burchard W, Ross-Murphy SB, editors. Physical networks, polymers and gels. Amsterdam: Elsevier; 1990.
[14] Drake MP, Veis A. Interchain interactions in collagen-fold formation. I. The kinetics of renaturation of gamma-gelatin. Biochemistry 1964;3:135–45.
[15] Harrington WF, Karr GM. Collagen structure in solution. II. Analysis of refolding kinetics in terms of nucleation and growth processes. Biochemistry 1970;9:3725–33.
[16] Hauschka PV, Harrington WF. Collagen structure in solution. III. Effect of cross-links on thermal stability and refolding kinetics. Biochemistry 1970;9:3734–45.
[17] Hauschka PV, Harrington WF. Collagen structure in solution. IV. Conformational properties of refolded cross-linked chains. Biochemistry 1970;9:3745–54.
[18] Hauschka PV, Harrington WF. Collagen structure in solution. V. Kinetic mechanism of refolding of cross-linked chains. Biochemistry 1970;9:3754–63.
[19] Eagland D, Pilling G, Wheeler RG. Studies of the collagen fold formation and gelation in solutions of a monodisperse alpha gelatin. Faraday Discussions of the Chemical Society 1974;57:181–200.
[20] Gornall JL, Terentjev EM. Helix–coil transition of gelatin: helical morphology and stability. Soft Matter 2008;4:544–9.
[21] Takayanagi S, Ohno T, Nagatsuka N, Okawa Y, Shiba F, Kobayashi H, et al. Effect of concentration and pH on sol–gel transition of gelatin. Journal of the Society of Photographic Science and Technology of Japan 2002;65:49–54.
[22] Bohidar HB, Jena SS. Kinetics of sol–gel transition in thermoreversible gelation of gelatin. Journal of Chemical Physics 1993;98:8970–7.
[23] Bachmann A, Kiefhaber T, Boudko S, Engel J, Bachinger HP. Collagen triple-helix formation in all-trans chains proceeds by a nucleation/growth mechanism with a purely entropic barrier. Proceedings of the National Academy of Sciences of the United States of America 2005;102:13897–902.
[24] Schonbrun J, Dill KA. Fast protein folding kinetics. Proceedings of the National Academy of Sciences of the United States of America 2003;100:12678–82.
[25] Shibayama M, Okamoto M. Dynamic light scattering study on gelatin aqueous solutions and gels. Journal of Chemical Physics 2001;115:4285–91.
[26] Olivares ML, Peirotti MB, Deiber JA. Analysis of gelatin chain aggregation in dilute aqueous solutions through viscosity data. Food Hydrocolloids 2006;20:1039–49.
[27] Zandi M, Mirzadeh H, Mayer C. Early stages of gelation in gelatin solution detected by dynamic oscillating rheology and nuclear magnetic spectroscopy. European Polymer Journal 2007;43:1480–6.
[28] Macsuga DD. Thermal transitions in gelatin: optical rotation and enthalpy changes. Biopolymers 1972;11:2521–32.
[29] Joly-Duhamel C, Hellio D, Djabourov M. All gelatin networks: 1. Biodiversity and physical chemistry. Langmuir 2002;18:7208–17.
[30] James HB, Wilmer LS. Thermal conductivity measurements of viscous liquids. Industrial and Engineering Chemistry 1955;47:289–93.
[31] Klech CM, Li XM. Consideration of drug load on the swelling kinetics of glassy gelatin matrices. Journal of Pharmaceutical Sciences 1990;79:999–1004.
[32] Hom FS, Veresh SA, Ebert WR. Soft gelatin capsules II: oxygen permeability study of capsule shells. Journal of Pharmaceutical Sciences 1975;64:851–7.
[33] Orakdogen N, Okay O. Correlation between crosslinking efficiency and spatial inhomogeneity in poly(acrylamide) hydrogels. Polymer Bulletin 2006;57:631–41.
[34] Orakdogen N, Okay O. Influence of the initiator system on the spatial inhomogeneity in acrylamide-based hydrogels. Journal of Applied Polymer Science 2007;103:3228–37.
[35] Liu RG, Oppermann W. Spatial inhomogeneities of polystrene gels prepared from semidilute solutions. Macromolecules 2006;39:4159–67.
[36] Norisuyea T, Masuia N, Kidaa Y, Ikutab D, Kokufutac E, Itod S, et al. Small angle neutron scattering studies on structural inhomogeneities in polymer gels: irradiation cross-linked gels vs chemically cross-linked gels. Polymer 2002;43:5289–97.

[37] Orakdogen N, Kizilay MY, Okay O. Suppression of inhomogeneities in hydrogels formed by free-radical crosslinking copolymerization. Polymer 2005;46:11407–15.
[38] Abdurrahmanoglu S, Okay O. Preparation of homogeneous hydrogels by controlling the crosslinker reactivity and availability. Journal of Macromolecular Science, Part A 2008;45:769–75.
[39] Andrade SR, Jardini AL, Maciel MRW, Maciel R. Numerical simulation of localized cure of thermosensitive resin during thermo stereolithography process (TSTL). Composites Science and Technology 2007;67:1666–73.
[40] Ellwood KRJ, Baldwin J, Bauer DR. Numerical simulation of thermal oxidation in automotive tires. Rubber Chemistry and Technology 2006;79:249–66.
[41] Ghoreishy MHR, Naderi G. Three-dimensional finite element modeling of rubber curing process. Journal of Elastomers and Plastics 2005;37:37–53.
[42] Jia YX, Sun S, Xue SX, Liu LL, Zhao GQ. Investigation of computer-aided engineering of silicone rubber vulcanizing (II) – finite element simulation of unsteady vulcanization field. Polymer 2002;43:7515–20.
[43] Jia YX, Sun S, Liu LL, Xue SX, Zhao GQ. Investigation of computer-aided engineering of silicone rubber vulcanizing (I) – vulcanization degree calculation based on temperature field analysis. Polymer 2003;44:319–26.
[44] Yang WH, Rao MA. Transient natural convection heat transfer to starch dispersion in a cylindrical container: numerical solution and experiment. Journal of Food Engineering 1998;36:395–415.
[45] Nielsen H, Marr BU, Hvidt S. Correlation between sagging and shear elasticity in pectin, gelatin and polyacrylamide gels. Carbohydrate Polymers 2001;45:395–401.
[46] Feng LG, Jia YX, Chen XL, An LJ. Finite element simulation of the physical gelation of rennet casein. Acta Polymerica Sinica 2008;6:529–36.
[47] Kong XQ. Applications of finite element method in heat transfer theory. 3rd ed. Beijing: Science Press; 1998.
[48] Joly-Duhamel C, Hellio D, Ajdari A, Djabourov M. All gelatin networks: 2. The master curve for elasticity. Langmuir 2002;18:7158–66.
[49] Yang SM, Tao WQ. Heat transfer. 4th ed. Beijing: Higher Education Press; 2006.